The control of by-product formation rates in photocatalytic hydrogen evolution reaction from organic substances over Pt/g–C$_3$N$_4$

Ksenia O. Potapenko[a], Egor E. Aydakov[b], Evgeny Y. Gerasimov[c], Ekaterina A. Kozlova[d]

Boreskov Institute of Catalysis, SB RAS, Novosibirsk, 630090, Russia

[a]potapenko@catalysis.ru, [b]e.ajdakov@g.nsu.ru, [c]gerasimov@catalysis.ru, [d]kozlova@catalysis.ru

Corresponding author: Ksenia O. Potapenko, potapenko@catalysis.ru

ABSTRACT The results on the photocatalytic activity of $0 - 2$ wt.% Pt/g-C$_3$N$_4$ in the hydrogen evolution reaction under visible light (430 nm) are presented. Triethanolamine (TEOA), glycerol, glucose and cellulose were used as electron donor. During the reaction, not only the target product, hydrogen, but also by-products of the reaction in the gas phase, namely CO and CO$_2$, were controlled. In order to study the chemical composition, microstructure and optical properties, the samples were investigated by XPS, TEM and diffuse reflection methods. The maximum hydrogen evolution rate obtained for 1 % Pt/g-C$_3$N$_4$ from TEOA solution was 3.96 μmol·min^{-1}, with a selectivity of 100 %. The use of glycerol and cellulose resulted in the production of syngas, and varying the platinum content allowed the selectivity of the process to vary (42.4 to 100 %). Glucose using led to the formation of a mixture of CO$_2$ and H$_2$ with a selectivity of 90 % or higher. In general, hydrogen-containing mixtures obtained using organic substrates can be further used in various applications.

KEYWORDS photocatalysis, hydrogen evolution, carbon nitride, triethanolamine, glycerol, cellulose, glucose, visible light

1. Introduction

Currently, one third of the world's energy is produced by burning coal, with coal-fired power plants emitting large amounts of greenhouse gases into the atmosphere [1]. With the depletion of the world's fossil fuel reserves and global warming, the search for alternative energy sources is an urgent task today [2, 3]. Solar energy is sustainable, renewable and more environmentally friendly energy source than conventional energy sources as it has no negative impact on the environment [4]. In recent times, there has been a worldwide trend to convert the inexhaustible energy of solar irradiation into useful products, such as hydrogen in the process of photocatalytic hydrogen production using semiconductor catalysts [5, 6]. However, the realization of such a kinetically slow process requires the development of materials active under visible irradiation, since the spectral range of solar irradiation consists more of visible light [7].

The most common photocatalyst is titanium dioxide, as they are commercially available (e.g. Degussa P25) and non-toxic [8, 9]. However, the application area in photocatalytic reactions is limited to the UV range. Graphitic carbon nitride, an n-type semiconductor, is a new generation photocatalyst because it is nontoxic, thermally stable, chemically stable in both alkaline and acidic media, and its band structure is suitable for the process of photocatalytic hydrogen evolution [10, 11]. However, the activity of pristine g-C$_3$N$_4$ in such a process is low due to the rapid recombination of electrons and holes [12]. Currently, several strategies have been proposed to increase the activity of graphitic carbon nitride, including doping with various heteroatoms [13, 14], deposition of co-catalysts [15–17], grinding of graphitic carbon nitride [18], surface engineering including nanosheet formation [19, 20], surface modification with acids [21], and so on. It is also interesting to modify the synthesis procedure, using different nitrogen-containing precursors, including combining them in different ratios [22]. For example, using a mixture of melamine and urea as precursors, a high surface area of g-C$_3$N$_4$ can be achieved due to the formation of a supramolecular melamine-cyanuric acid complex during synthesis [22].

Platinum nanoparticles are known to increase photocatalytic activity. In this case, the formation of Schottky barrier between the metal (Pt, Au and Ag) and semiconductor (g-C$_3$N$_4$) is observed, which leads to an increase in photocatalytic activity due to an increase in the lifetime of electron-hole pairs [9]. Noble metal nanoparticles "capture" electrons in the conduction band of the semiconductor, which further reduce protons to form hydrogen. In addition, the work of electron

escape from vacuum for Pt in the metallic state is 5.40 eV, which is the highest value among noble metals [10]. Based on this, the choice of co-catalyst (Pt) for surface modification of graphitic carbon nitride was carried out.

When carrying out the photocatalytic process in solutions of organic compounds, an important task is to analyze all products in the gas phase, such as CO and CO_2, which can be formed as a result of complete or partial oxidation of substrates. The composition of the resulting hydrogen-containing mixtures influences their further applications.

In this work, we have shown for the first time the complex influence of the mass fraction of platinum deposited on the surface of graphitic carbon nitride and the electron donor used on the activity and selectivity of photocatalytic hydrogen evolution under visible light irradiation (430 nm). Not only model substrates – triethanolamine, glycerol, but also components of plant biomass – glucose and cellulose – were used as electron donors. The novelty of the work consists in determining the correlation between the electron donor, the mass fraction of platinum $Pt/g-C_3N_4$ and the selectivity of the photocatalytic hydrogen evolution reaction.

2. Materials and methods

2.1. Photocatalyst synthesis

A method to obtain graphitic carbon nitride is described in [22]. Briefly, the required amount of a mixture of melamine (Sigma-Aldrich, USA, 99 %) and urea (Acros Organics, USA, 99 %) in a mass ratio of 1:3 was placed in a crucible, then in a muffle oven with subsequent heating at a rate of 10 °C/min to 525 °C, held for 1 hour. The resulting powder was cooled to room temperature, grinded and used further.

The deposition of platinum particles was carried out by soft chemical reduction method. 500 mg of prepared $g-C_3N_4$ was placed in a glass beaker, suspended in a small amount of distilled water, a solution of 0.1 M H_2PtCl_6 (Reakhim, Russia, 98 %) was added dropwise and stirred for an hour. Then an excess of 0.1 M $NaBH_4$ solution was added and stirred for one hour. The precipitate was washed several times and then dried at 50 °C for 3 hours. The mass fraction of deposited platinum particles was varied during the synthesis. The catalysts were denoted by x % $Pt/g-C_3N_4$, where $x = 0.1, 0.5, 1, 2$.

2.2. Photocatalyst characterization

The photocatalysts were characterized by physicochemical methods of investigation, including X-ray photoelectron spectroscopy (XPS), transmission electron microscopy (TEM), diffuse reflectance electron spectroscopy (DRES) and UV-vis spectroscopy.

The chemical composition of the sample was investigated by X-ray photoelectron spectroscopy (XPS) on an electron spectrometer of SPECS SurfaceNanoAnalysisGmbH (Germany). The spectrometer was equipped with a PHOIBOS-150-MCD-9 hemispherical analyzer, XR-50 X-ray characteristic radiation source with double Al/Mg anode. Non-monochromatized radiation Al$K\alpha$ ($h\nu = 1486.61$ eV) was used to record the spectra. The position of the peak corresponding to the carrier was used to account for the charging effect of the samples (Table 1). Relative concentrations of elements in the analysis zone were determined on the basis of integral intensities of the XPS peaks taking into account the photoionization cross section of the corresponding terms. For detailed analysis, decomposition of spectra into individual components was used [23]. Accordingly, after background subtraction using the Shirley method [24], the experimental curve was decomposed into a number of lines corresponding to the photoemission of electrons from atoms in different chemical environments. The data were processed using the CasaXPS program package [25]. The shape of the peaks was approximated by a symmetric function obtained by summation of the Gauss and Lorentz functions.

TABLE 1. Relative atomic concentrations of elements in the near-surface layer of the studied catalysts

Sample	[N]/[C]	[Pt]/[C]	%, Pt^0	%, Pt^{2+}	[O_x]/[C]	[Na]/[C]
0.1 % $Pt/g-C_3N_4$	1.35	0.001	68	32	0.15	0.03
0.5 % $Pt/g-C_3N_4$	1.33	0.004	83	17	0.18	0.03
1 % $Pt/g-C_3N_4$	1.36	0.008	85	15	0.16	0.03
2 % $Pt/g-C_3N_4$	1.33	0.008	82	18	0.20	0.03

*[C] – carbon in the C–N=C carrier (288.1 eV);

**[Carbon] – surface carbon of C=C (284.9 eV);

***[O_x] – surface oxygen-containing impurities.

The microstructure of the photocatalysts was studied by transmission electron microscopy (TEM) using a ThemisZ microscope (Thermo Fisher Scientific, USA) at an accelerating voltage of 200 kV.

The UV-vis diffuse reflectance spectra were obtained with the use of Shimadzu UV2501 PC (Shimadzu, Kyoto, Japan) spectrophotometer with an ISR-240A diffuse reflectance attachment in the wavelength range from 400 to 850 nm.

2.3. Photocatalytic experiments

The photocatalytic hydrogen evolution reaction was carried out in the reactor shown in Fig. 1. 50 mL of electron donor (10 vol.% triethanolamine (AO Base #1 Chemicals, h.), 0.4 M glycerol (AO Base #1 Chemicals, h.), 0.2 M α-D(+)-glucose (Acros Organics, 98 %), 3 M α-cellulose (Sigma)+ 0.1 M NaOH (Thermo Scientific, 98.5 %), and 25 mg of catalyst, which was pretreated in an ultrasonic bath for 10 minutes. The reactor was then purged with argon for 20 minutes. An LED with a wavelength of 430 nm was used as the light source. The gaseous reaction products including H_2, CO, CO_2 were analyzed using a CHROMOS GC-1000 gas chromatograph equipped with a methanator and a thermal conductivity detector.
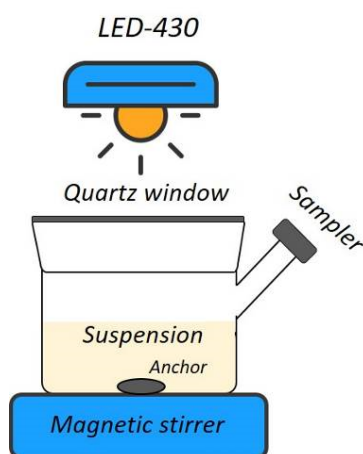

FIG. 1. Schematic representation of the reactor for photocatalytic hydrogen evolution reaction

In addition to the photocatalytic hydrogen evolution rate, the apparent quantum efficiency (AQE) was calculated using the formula

$$AQE = \frac{2W(\mathrm{H}_2)}{N_f},$$

where $W(\mathrm{H}_2)$ is the hydrogen evolution rate, mol/min; N_f is the photon flux, mol/min.

3. Results and discussion

3.1. Photocatalyst characterization

All investigated catalysts were characterized by X-ray photoelectron spectroscopy. Peaks corresponding to Pt, N, C, Na, and O were detected in the XPS spectra of the catalysts. The relative concentrations (atomic ratios) of elements in the near-surface layer of the catalysts determined from the XPS data are presented in Table 1. The values of binding energies of C$1s$, N$1s$, Pt$4f_{7/2}$ peaks are presented in Table 2. It is important to note that the peak in the C$1s$ spectrum of carbon corresponding to the spectrum of the carrier (g-C_3N_4) was chosen for calibration of the binding energy scale. At the same time, the obtained values of binding energy of the C$1s$ carbon peak included in the carbon impurities on the catalyst surface lie in the range of 284.8 – 285.0 eV (Table 2), which confirms the correctness of the calibration.

According to the data presented in Table 1, platinum in the investigated samples is represented by two forms: oxidized (Pt^{2+}) and reduced (Pt^0), and with the increase of its content in the samples, the fraction of metallic platinum increases and reaches 85 % for the sample 1 % Pt/g-C_3N_4.

Figure 2 shows the C$1s$ and N$1s$ spectra of the catalysts. The C$1s$ spectrum is well described by two peaks with binding energies around 284.9 and 288.1 eV. The first peak is characteristic of carbon-containing impurities present on the surface of the catalysts. The second peak is characteristic of C$1s$ g-C_3N_4 and corresponds to carbon forming bonds with nitrogen atoms in the g-C_3N_4 structure [26, 27]. In the case of the N$1s$ spectrum, 4 peaks with binding energies around 398.6, 399.9, 401.0, and 404.5 eV are observed. According to literature data, the first peak refers to nitrogen atoms forming a C–N=C bond, the second peak refers to form a bond with three carbon atoms N–(C)$_3$, and the third peak refers to N–H terminal groups [26, 27]. The fourth peak corresponds to an excited π-bond.

Figure 3 shows the Pt$4f$ spectra of the studied catalysts. The $4f$-level of platinum is known to split into two sublevels Pt$4f_{7/2}$ and Pt$4f_{5/2}$ due to spin-orbit interaction, the spin-orbit splitting of which is 3.33 eV. In the literature, for massive

TABLE 2. Values of C*1s*, N*1s* and Pt*4f*$_{7/2}$ binding energies. The spectra are calibrated on the C*1s* line (EeSv = 288.1 eV)

Sample	C*1s*		N*1s*				Pt*4f*$_{7/2}$	
	C=C, 284.9 eV	C–N=C, 288.1 eV	C–N=C, 398.6 eV	(C)$_3$–N, 399.9 eV	N–H, 401.0 eV	π, 404.5 eV	Pt^0, 71.0 eV	Pt^{2+}, 72.9 eV
0.1 % Pt/ g-C$_3$N$_4$	40	60	72	14	10	4	68	32
0.5 % Pt/ g-C$_3$N$_4$	42	58	73	14	10	3	83	17
1 % Pt/ g-C$_3$N$_4$	40	60	72	14	10	4	85	15
2 % Pt/ g-C$_3$N$_4$	47	53	72	14	10	4	82	18
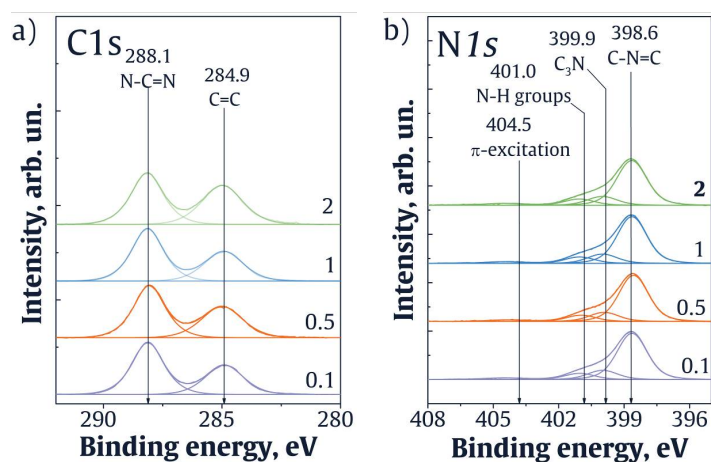
FIG. 2. C*1s* and N*1s* spectra of the carrier. The N*1s* spectrum is normalized by the integral intensity of the C*1s* peak corresponding to the carrier spectrum (g-C$_3$N$_4$)

metallic platinum samples, the binding energy of Pt*4f*$_{7/2}$ is 71.1 – 71.6 eV [28]. In turn, for massive PtO, PtO$_2$ and Pt(OH)$_4$, the values of Pt*4f*$_{7/2}$ binding energy lie in the range of 72.3 – 73.0, 74.0 – 74.1 and 74.2 – 74.4 eV [29–31]. In the case of the investigated catalysts, the Pt*4f* spectrum is approximated by two Pt*4f*$_{7/2}$–Pt*4f*$_{7/2}$ doublets with Pt*4f*$_{7/2}$ binding energies around 70.8 – 71.0 and 72.8 – 72.9 eV, respectively. These doublets are related to platinum in the metallic state as well as to platinum in the oxidized state, Pt^{2+}.
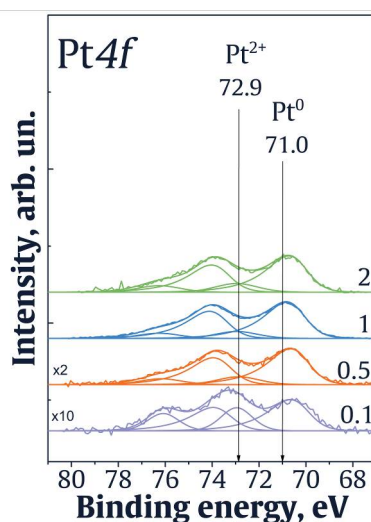
FIG. 3. Pt*4f* spectra of the investigated catalysts. The spectra were normalized by the integral intensity of the C*1s* peak corresponding to the spectrum of the g-C$_3$N$_4$

The microstructure of the photocatalysts was studied by transmission electron microscopy (TEM). For the 0.1 % Pt/g-C$_3$N$_4$ catalyst, small single Pt particles of size 2.1 ± 0.9 nm uniformly distributed on the surface of graphitic carbon nitride g-C$_3$N$_4$ were observed. With the increase in platinum loading (0.5 – 2 %), agglomeration of Pt particles is observed. Thus, in the case of 0.5 % Pt/g-C$_3$N$_4$ the size of agglomerates is about 12 nm, and for 2 % Pt/g-C$_3$N$_4$ it is about 50 nm. It should be noted that according to the particle size distribution (Fig. 4), the average particle size does not practically change with increasing platinum loading. The agglomeration of platinum particles may be related to the supersaturation of the graphitic carbon nitride surface by the platinum precursor H$_2$PtCl$_6$. The literature indicates that when using the precursor Pt(IV), namely H$_2$PtCl$_6$, there is no formation of π-complexes with carbon-containing surface, and therefore leads to a high degree of agglomeration of platinum particles [32].
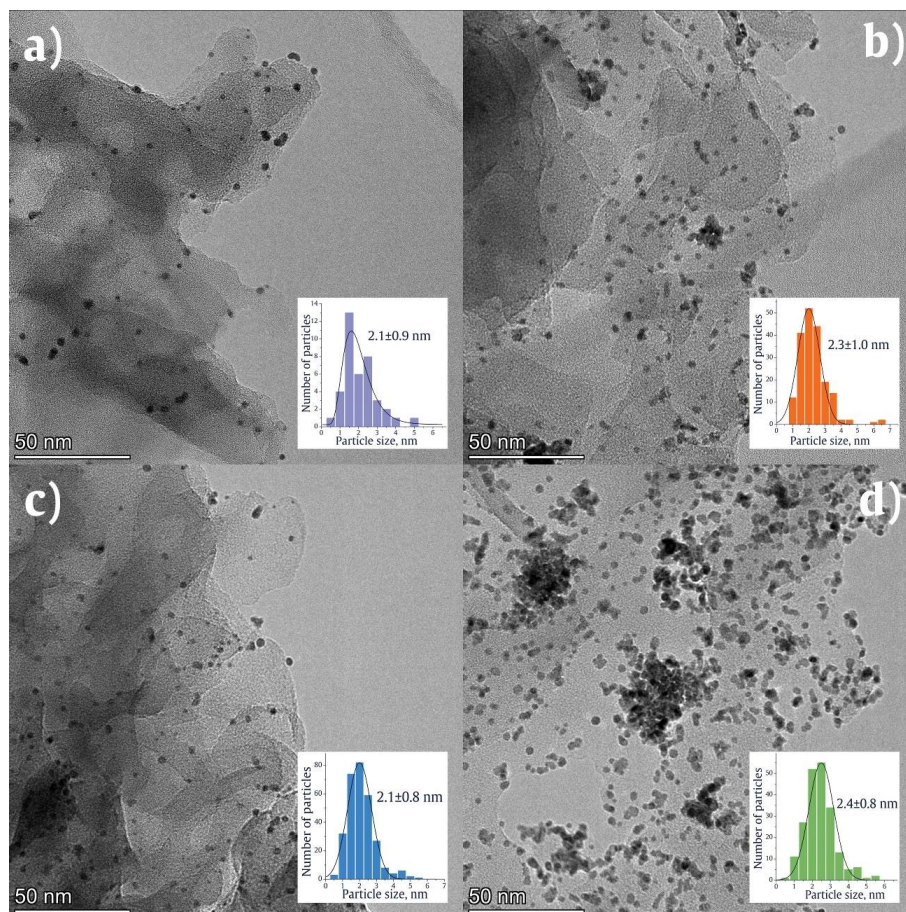

FIG. 4. SEM images and particle size distribution for 0.1 (a); 0.5 (b); 1 (c); 2 (d) % Pt/g-C$_3$N$_4$ catalysts

The diffuse reflectance spectra for $0 - 2$ % Pt/g-C$_3$N$_4$ catalysts are shown in Fig. 5. Light absorption is shown to increase in the region of $450 - 800$ nm when platinum particles are deposited on the surface of graphitic carbon nitride g-C$_3$N$_4$, which is due to the effect of surface plasmon resonance of Pt particles (Fig. 5a). The determined bandgap energies of all catalysts was carried out in Tauc coordinates (Fig. 5b) by extrapolating the dependence of $(F(R) \cdot E)^{0.5}$ of E. For g-C$_3$N$_4$, 0.1 % Pt/g-C$_3$N$_4$, 0.5 % Pt/g-C$_3$N$_4$, 1 % Pt/g-C$_3$N$_4$, 2 % Pt/g-C$_3$N$_4$, the bandgap energies were 2.62, 2.69, 2.66, 2.63, 2.66 eV, respectively.

3.2. Photocatalytic activity

All synthesized Pt/g-C$_3$N$_4$ catalysts were tested in the reaction of photocatalytic hydrogen evolution from aqueous solutions of electron donors: 10 vol.% triethanolamine, 0.4 M glycerol, 0.2 M α-D(+)-glucose (glucose), 3 M α-cellulose (cellulose) + 0.1 M NaOH. Summary on the rates of formation of photocatalytic reaction products for all catalysts from aqueous solutions of electron donors is presented in Table 3.

When studying the dependence of the hydrogen evolution rate on the platinum content on the surface of graphitic carbon nitride, a dome-shaped dependence was obtained in the case of using TEOA, glycerol and glucose as electron donors, as shown in Fig. 6. An increase in the platinum content ($0.1 - 1$ %) on the surface of graphitic carbon nitride g-C$_3$N$_4$ leads to an increase in the number of adsorption centers for organic molecules [33, 34] and an increase in metal-semiconductor contacts, due to which the lifetime of photogenerated charges increases [35]. On the other hand, high metal concentration (2 %) hinders the light absorption and also limits the adsorption of organic electron donors. When
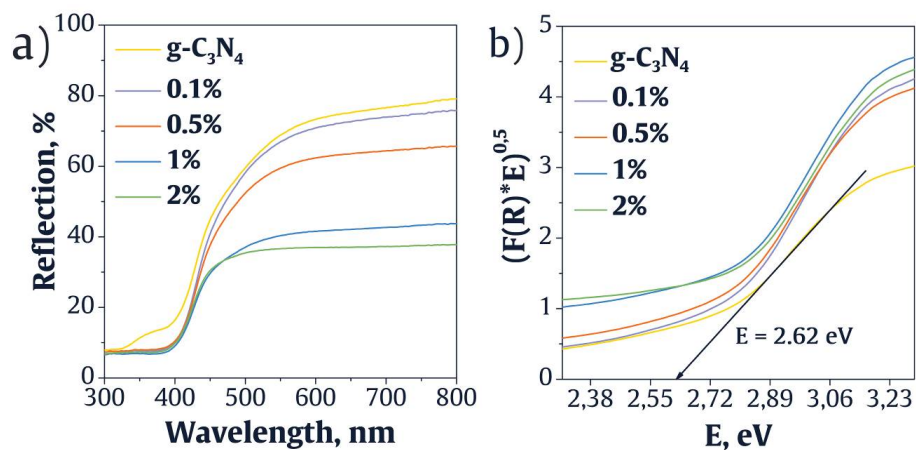
FIG. 5. Electronic diffuse reflectance spectra of UV-visible spectroscopy (a) and plot of the dependence of $(F(R) \cdot E)^{0.5}$ on E (b)

TABLE 3. Summary table of the rates of formation of photocatalytic reaction products for $0 - 2$ % Pt/g-C_3N_4 catalysts from aqueous solutions of electron donors

Electron donor	x % Pt/ g-C_3N_4	W			AQE, %
		H_2, μmol·min^{-1}	CO, nmol·min^{-1}	CO_2, nmol min^{-1}	
TEOA	0.1	0.7	0	0	0.5
	0.5	1.9			1.2
	1	4.0			2.6
	2	2.8			1.8
Glycerol	0.1	0.1	1.4	0	<0.1
	0.5	0.2	2.2		0.1
	1	0.3	0.2		0.2
	2	0.1	0.4		<0.1
Glucose	0.1	0.06	0	0.4	<0.1
	0.5	0.03		3.6	<0.1
	1	0.2		15.2	0.1
	2	0.1		10.0	<0.1
Cellulose	0.1	0.0008	0.5	0	<0.1
	0.5	0.006	1.3		<0.1
	1	0.02	1.0		<0.1
	2	0.07	1.0		<0.1

the mass fraction of Pt increases, according to TEM images (Fig. 4), nanoparticles begin to aggregate, which is one of the possible reasons for the decrease in catalytic activity. According to the XPS results (Table 1), the highest proportion of metallic platinum, namely 85 %, is observed for the 1 % Pt/g-C_3N_4 catalyst, which in turn is the most active in the process of hydrogen evolution for all the substrates used. Thus, the separation of photogenerated electrons and holes proceeds more efficiently with higher amounts of reduced platinum (Pt^0). In general, the observed dependence is a combination of several factors: the platinum state (oxidized Pt^{2+}, reduced Pt^0) and its content on the surface of graphitic carbon nitride g-C_3N_4, as well as the distribution of platinum particles on the catalyst surface. The maximum rate of hydrogen evolution was observed from TEOA solution (10 vol.%) when 1 % Pt/g-C_3N_4 was added and was 3.96 μmol·min^{-1}.
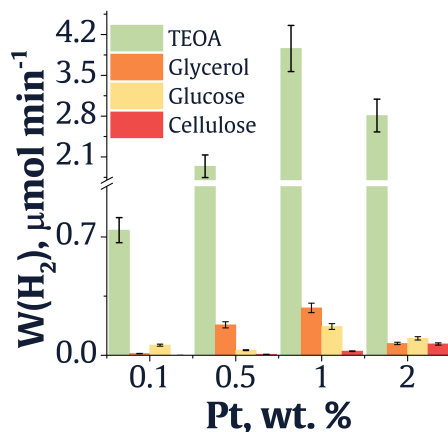

FIG. 6. Dependence of hydrogen evolution rate on Pt loading on g-C_3N_4. Experimental conditions: m(catalyst) $=$ 25 mg, V(suspension) $=$ 50 ml, λ $=$ 430 nm, t(reaction) $=$ 90 min, C(TEOA) $=$ 10 vol.%; C(Glycerol) $=$ 0.4 M; C(Glucose) $=$ 0.2 M; C(Cellulose) $=$ 3 M

In addition to the identification of the target product, hydrogen, the presence of carbon monoxide and carbon dioxide in the gas phase was additionally analyzed. The formation of such products can occur in the process of complete or partial oxidation of organic substrates. The dependence of the product ratio on the mass fraction of platinum on the surface of graphitic carbon nitride using TEOA (Fig. 7a), glycerol (Fig. 7b), glucose (Fig. 7c), cellulose (Fig. 7d) as electron donors is presented in Fig. 7.

When the photocatalytic hydrogen evolution reaction is carried out from triethanolamine solution, the formation of pure hydrogen is observed. Impurity-free hydrogen can be used to power fuel cells, since proton exchange membranes inside fuel cells are known to undergo CO poisoning [36]. Probably, during phototocatalytic transformations triethanolamine is oxidized to glyceraldehyde by photogenerated holes, while complete oxidation does not occur.

The use of glycerol and cellulose results in a mixture consisting of hydrogen and carbon monoxide. A general pattern is observed: the mass content of platinum on the surface of graphitic carbon nitride strongly influences the distribution of reaction products, and hence the selectivity for CO and H_2. In particular, in cellulose solution at increasing of Pt loading mainly reaction product in gas phase is hydrogen, while for catalysts 0.1 % Pt/g-C_3N_4 and 0.5 % Pt/g-C_3N_4 the CO:H_2 ratio is 1:1.3 and 1:3.7, respectively. This result can be explained by the fact that Pt is a catalyst for hydrogenation, so with the increase of its loading the amount of CO decreases both in the case of the reaction in glycerol solution and in cellulose solution [37,38]. Hydrogenation of carbon monoxide to various reaction products (probably light hydrocarbons) takes place [38].

Varying the ratio of gases in the carbon monoxide:hydrogen mixture makes it possible to obtain products for the production of synthetic fuel (synfuel). Synthesis of synfuel is extremely important because such combustible liquids are used as motor fuel in internal combustion engines [39]. The combustion of synfuel proceeds without the formation of soot and NO$_x$, etc [40]. Thus, for production of ethylene glycol and vinyl acetate synthesis gas is used in the ratio 1:1 (CO:H_2), and for realization of steam conversion process the ratio 1:2,2 (CO:H_2) is necessary [41].

As for the products of substrate oxidation in the liquid phase, according to literature data, in the case of glycerol, oxidation proceeds through the C–C bond, which ultimately leads to the formation of the main product C_2 in the liquid phase – glycolic acid [42]. This is explained by the fact that irradiation of the photocatalyst results in the formation of a large number of reactive oxygen species, which induce the conversion of the intermediate product, glyceraldehyde, into glycolic acid. The formation of glyceric acid and dihydroxyacetone is also observed [43]. When carrying out the photocatalytic reaction in a weakly alkaline cellulose solution, the mechanism of oxidation of the organic substrate is more complex, since such a process can proceed in several directions simultaneously. Thus, oxidation of primary alcohol groups (C_6) with formation of aldehyde and then carboxyl groups; secondary alcohol groups (C_2 and C_3) with formation of ketones and their subsequent oxidation to carboxyl groups is possible [44]. In general, glycerol and cellulose are resistant to oxidation by photogenerated holes, so complete oxidation of substrates does not occur.
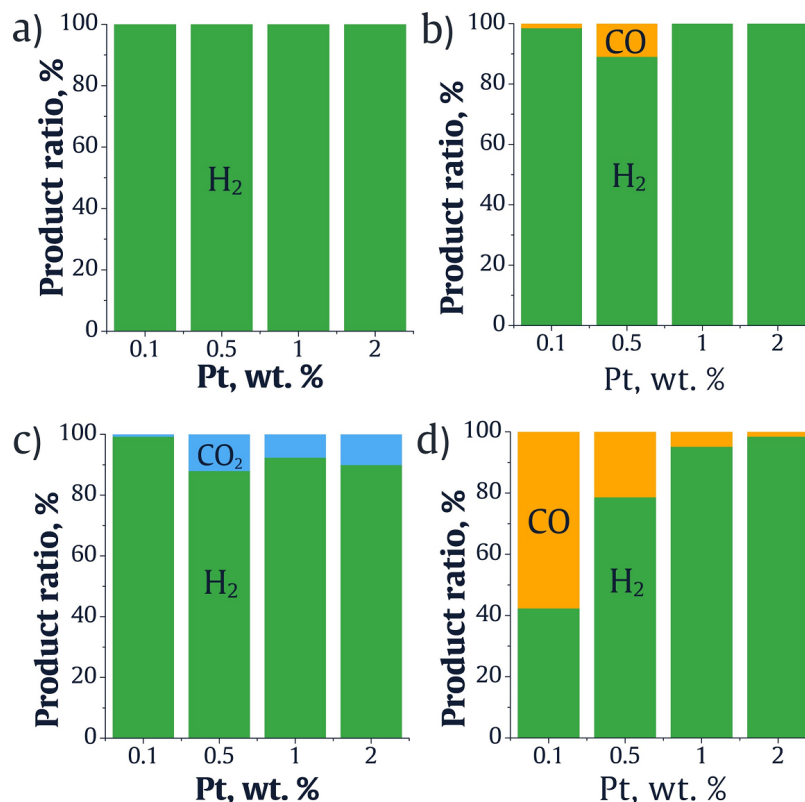
FIG. 7. Distribution of products in the gas phase as a function of platinum loading for the Pt/g-C$_3$N$_4$ catalyst when the process is carried out in a solution of TEOA (a), glycerol (b), glucose (c), cellulose (d). Reaction conditions: m(catalyst) = 25 mg, V(suspension) = 50 mL, λ = 430 nm, t(reaction) = 90 min, C(TEOA) = 10 vol.%; C(Glycerol) = 0.4 M; C(Glucose) = 0.2 M; C(Cellulose) = 3 M

Complete oxidation of glucose proceeds relatively easily even in anaerobic environment, so a mixture of CO$_2$ and H$_2$ was detected in gas phase analysis for all catalysts. The selectivity is almost independent of the amount of platinum deposited on the surface of g-C$_3$N$_4$. The mixture of gases obtained in this case can be converted into carbon monoxide, which, as previously mentioned, is a valuable product for organic synthesis. It is also possible to obtain methane by hydrogenation of CO$_2$. From the thermodynamic point of view, the more favorable product of glucose oxidation in the liquid phase at high temperatures is lactic acid. On the contrary, lower temperatures are favorable for the production of formate [45]. The photocatalytic reactions presented in this work were carried out at room temperature, hence, the main oxidation product in the liquid phase is probably formic acid.

When comparing the results obtained with literature data (Table 4), it was found that the values of the rates of formation of photocatalytic reaction products exceed or are on par with already published data. It should be noted that there are very few papers devoted to photocatalytic hydrogen evolution with simultaneous detection of not only the target product – hydrogen, but also detection of reaction by-products, including CO and CO$_2$. At the same time, there are no papers in which low-soluble biomass components, such as cellulose, are used as electron donors.

4. Conclusion

In this work, a series of photocatalysts based on graphitic carbon nitride g-C$_3$N$_4$ with subsequent surface modification with Pt particles (0 – 2 wt.%) were synthesized. The samples were tested in the reaction of photocatalytic hydrogen evolution under visible irradiation (430 nm) not only from model substrates, including triethanolamine, glycerol, but also from plant biomass components – glucose and cellulose. The dependence of catalyst activity on platinum content was a combination of several factors, namely: the state of platinum: Pt^{2+}, Pt^0, and the ratio of these forms; the distribution of platinum-containing particles on the catalyst surface: single particles or agglomerates. The maximum hydrogen evolution rate was observed when 1 %Pt/g-C$_3$N$_4$ was added from triethanolamine solution and amounted to 9.6 mmol·g^{-1}·h^{-1} (AQE = 2.6 %). When studying the influence of Pt loading and the nature of electron donor on the selectivity of reaction product formation in the gas phase, it was found that using cellulose and glycerol, it is possible to obtain synthesis gas in different CO:H$_2$ ratios by varying the Pt loading. Carrying out the target reaction in TEOA solution resulted in the production of high-purity hydrogen. The formation of a mixture of CO$_2$ and H$_2$ occurred when glucose was used as an electron donor.

TABLE 4. Comparison of the obtained values of formation rates of reaction products, including H_2, CO and CO_2, of the synthesized sample with literature data

Catalyst	Light source	Electron donor	$W(H_2)$, $\mu mol \cdot g^{-1} \cdot h^{-1}$	$W(CO)$, $\mu mol \cdot g^{-1} h^{-1}$	$W(CO_2)$, $\mu mol \cdot g^{-1} h^{-1}$	Ref.
$Cd_{0.8}Zn_{0.2}S/2$ wt.% Au/gC_3N_4	Xe lamp $\lambda > 420$ nm	0.1 M glucose	123.21	8.1	38.2	[46]
0.5 wt.% Pt / TiO_2/g-C_3N_4	LED $\lambda = 450$ nm	10 vol.% TEOA	5100	0	2100	[47]
		10 vol.% glycerol	860	0	2100	
1 wt.% Pt/g-C_3N_4	LED $\lambda = 430$ nm	10 vol.% TEOA	9600	0	0	This work
		0.4 M glycerol	720	0.5	0	
		0.2 M glucose	480	0	36.5	
		3 M cellulose	48	2.4	0	

References

[1] Li J., Xin Y., Hu B., Zeng K., Wu Z., Fan S., Li Y., Chen Y., Wang S., Wang J., et al. Safety and Thermal Efficiency Performance Assessment of Solar Aided Coal-Fired Power Plant Based on Turbine Steam Double Reheat. *Energy*, 2021, **226**, 120277.

[2] Alola A.A., Olanipekun I.O., Shah M.I. Examining the Drivers of Alternative Energy in Leading Energy Sustainable Economies: The Trilemma of Energy Efficiency, Energy Intensity and Renewables Expenses. *Renew. Energy*, 2023, **202**, P. 1190–1197.

[3] Zlotin S.G., Egorova K.S., Ananikov V.P., Akulov A.A., Varaksin M.V., Chupakhin O.N., Charushin V.N., Bryliakov K.P., Averin A.D., Beletskaya I.P., et al. The Green Chemistry Paradigm in Modern Organic Synthesis. *Russ. Chem. Rev.*, 2023, **92**, RCR5104.

[4] Azam M.S., Bhattacharjee A., Hassan M., Rahaman M., Aziz S., Ali Shaikh M.A., Islam M.S. Performance Enhancement of Solar PV System Introducing Semi-Continuous Tracking Algorithm Based Solar Tracker. *Energy*, 2024, **289**, 129989.

[5] Xu F., Weng B. Photocatalytic Hydrogen Production: An Overview of New Advances in Structural Tuning Strategies. *J. Mater. Chem. A*, 2023, **11**, P. 4473–4486.

[6] Chu X., Sathish C.I., Yang J.H., Guan X., Zhang X., Qiao L., Domen K., Wang S., Vinu A., Yi J. Strategies for Improving the Photocatalytic Hydrogen Evolution Reaction of Carbon Nitride-Based Catalysts. *Small*, 2023, **19**, 2302875.

[7] Li T., Tsubaki N., Jin Z. S-Scheme Heterojunction in Photocatalytic Hydrogen Production. *J. Mater. Sci. Technol.*, 2024, **169**, P. 82–104.

[8] Dorosheva I.B., Vokhmintsev A.S., Weinstein I.A., Rempel A.A. Induced Surface Photovoltage in TiO_2 Sol-Gel Nanoparticles. *Nanosystems: Phys. Chem. Math.*, 2023, **14**, P. 447–453.

[9] Kozlova E.A., Valeeva A.A., Sushnikova A.A., Zhurenok A.V., Rempel A.A. Photocatalytic Activity of Titanium Dioxide Produced by High-Energy Milling. *Nanosystems: Phys. Chem. Math.*, 2022, **13**, P. 632–639.

[10] Maeda K., Wang X., Nishihara Y., Lu D., Antonietti M., Domen K. Photocatalytic Activities of Graphitic Carbon Nitride Powder for Water Reduction and Oxidation under Visible Light. *J. Phys. Chem. C*, 2009, **113**, P. 4940–4947.

[11] Gao F., Xiao H., Yang J., Luan X., Fang D., Yang L., Zi J., Lian Z. Modulation of Electronic Density in Ultrathin G-C_3N_4 for Enhanced Photocatalytic Hydrogen Evolution through an Efficient Hydrogen Spillover Pathway. *Appl. Catal. B Environ.*, 2024, **341**, 123334.

[12] Fu J., Yu J., Jiang C., Cheng B. G-C_3N_4-Based Heterostructured Photocatalysts. *Adv. Energy Mater.*, 2018, **8**, 1701503.

[13] Feng C., Tang L., Deng Y., Wang J., Liu Y., Ouyang X., Yang H., Yu J., Wang J. A Novel Sulfur-Assisted Annealing Method of g-C_3N_4 Nanosheet Compensates for the Loss of Light Absorption with Further Promoted Charge Transfer for Photocatalytic Production of H_2 and H_2O_2. *Appl. Catal. B Environ.*, 2021, **281**, 119539.

[14] Zou J., Liao G., Jiang J., Xiong Z., Bai S., Wang H., Wu P., Zhang P., Li X. In-Situ Construction of Sulfur-Doped g-C_3N_4/Defective g-C_3N_4 Isotype Step-Scheme Heterojunction for Boosting Photocatalytic H_2 Evolution. *Chinese J. Struct. Chem.*, 2022, **41**, P. 2201025–2201033.

[15] Zhang G., Lan Z.A., Wang X. Surface Engineering of Graphitic Carbon Nitride Polymers with Cocatalysts for Photocatalytic Overall Water Splitting. *Chem. Sci.*, 2017, **8**, P. 5261–5274.

[16] Rosman N.N., Yunus R.M., Shah N.R.A.M., Shah R.M., Arifin K., Minggu L.J., Ludin N.A. An Overview of Co-Catalysts on Metal Oxides for Photocatalytic Water Splitting. *Int. J. Energy Res.*, 2022, **46**, P. 11596–11619.

[17] Kharina S.N., Kurenkova A.Y., Saraev A.A., Gerasimov E.Y., Kozlova E.A. Copper-Modified g-C_3N_4/TiO_2 Nanostructured Photocatalysts for H_2 Evolution from Glucose Aqueous Solution. *Nanosystems: Phys. Chem. Math.*, 2024, **15**, P. 388–397.

[18] Chebanenko M.I., Lebedev L.A., Tenevich M.I., Stovpiaga E.Y., Popkov V.I. Planetary Grinding's Impact on the Structure and Photocatalytic Characteristics of Urea-Derived g-C_3N_4 Nanocrystals. N*anosystems: Phys. Chem. Math.*, 2023, **14**, P. 705–712.

[19] Huang D., Li Z., Zeng G., Zhou C., Xue W., Gong X., Yan X., Chen S., Wang W., Cheng M. Megamerger in Photocatalytic Field: 2D g-C_3N_4 Nanosheets Serve as Support of 0D Nanomaterials for Improving Photocatalytic Performance. *Appl. Catal. B Environ.*, 2019, **240**, P. 153–173.

[20] Chen L., Maigbay M.A., Li M., Qiu X. Synthesis and Modification Strategies of G-C_3N_4 Nanosheets for Photocatalytic Applications. *Adv. Powder Mater.*, 2024, **3**, 100150.

[21] Liu C., Jing L., He L., Luan Y., Li C. Phosphate-Modified Graphitic C_3N_4 as Efficient Photocatalyst for Degrading Colorless Pollutants by Promoting O_2 Adsorption. *Chem. Commun.*, 2014, **50**, P. 1999–2001.

[22] Potapenko K.O., Cherepanova S.V., Kozlova E.A. A New Strategy for the Synthesis of Highly Active Catalysts Based on G-C_3N_4 for Photocatalytic Production of Hydrogen under Visible Light. *Dokl. Phys. Chem.*, 2023, P. 1–9.

[23] Scofield J.H. Hartree-Slater Subshell Photoionization Cross-Sections at 1254 and 1487 EV. *J. Electron Spectros. Relat. Phenomena*, 1976, **8**, P. 129–137.

[24] Shirley D.A. High-Resolution X-Ray Photoemission Spectrum of the Valence Bands of Gold. *Phys. Rev. B*, 1972, **5**, 4709.

[25] Fairley N. URL: www.casaxps.com.

[26] Dong F., Zhao Z., Xiong T., Ni Z., Zhang W., Sun Y., Ho W.K. In Situ Construction of G-C_3N_4/g-C_3N_4 Metal-Free Heterojunction for Enhanced Visible-Light Photocatalysis. *ACS Appl. Mater. Interfaces*, 2013, **5**, P. 11392–11401.

[27] Liu H., Chen D., Wang Z., Jing H., Zhang R. Microwave-Assisted Molten-Salt Rapid Synthesis of Isotype Triazine-/Heptazine Based g-C_3N_4 Heterojunctions with Highly Enhanced Photocatalytic Hydrogen Evolution Performance. *Appl. Catal. B Environ.*, 2017, **203**, P. 300–313.

[28] Tenney S.A., He W., Ratliff J.S., Mullins D.R., Chen D.A. Characterization of Pt-Au and Ni-Au Clusters on TiO_2(110). *Top. Catal.*, 2011, **54**, P. 42–55.

[29] Barr T.L. An ESCA Study of the Termination of the Passivation of Elemental Metals. *J. Phys. Chem.*, 1978, **82**, P. 1801–1810.

[30] Bernsmeier D., Sachse R., Bernicke M., Schmack R., Kettemann F., Polte J., Kraehnert R. Outstanding Hydrogen Evolution Performance of Supported Pt Nanoparticles: Incorporation of Preformed Colloids into Mesoporous Carbon Films. *J. Catal.*, 2019, **369**, P. 181–189.

[31] Gołabiewska A., Lisowski W., Jarek M., Nowaczyk G., Zielińska-Jurek A., Zaleska A. Visible Light Photoactivity of TiO_2 Loaded with Monometallic (Au or Pt) and Bimetallic (Au/Pt) Nanoparticles. *Appl. Surf. Sci.*, 2014, **317**, P. 1131–1142.

[32] Maillard F., Schreier S., Hanzlik M., Savinova E.R., Weinkauf S., Stimming U. Influence of Particle Agglomeration on the Catalytic Activity of Carbon-Supported Pt Nanoparticles in CO Monolayer Oxidation. *Phys. Chem. Chem. Phys.*, 2005, **7**, P. 385–393.

[33] Vorontsov A.V., Stoyanova I.V., Kozlov D.V., Simagina V.I., Savinov E.N. Kinetics of the Photocatalytic Oxidation of Gaseous Acetone over Platinized Titanium Dioxide. *J. Catal.*, 2000, **189**, P. 360–369.

[34] Lam S.W., Chiang K., Lim T.M., Amal R., Low G.K.C. The Effect of Platinum and Silver Deposits in the Photocatalytic Oxidation of Resorcinol. *Appl. Catal. B Environ.*, 2007, **72**, P. 363–372.

[35] Kozlova E.A., Parmon V.N. Heterogeneous Semiconductor Photocatalysts for Hydrogen Production from Aqueous Solutions of Electron Donors. *Russ. Chem. Rev.*, 2017, **86**, P. 870–906.

[36] Mazumder V., Lee Y., Sun S. Recent Development of Active Nanoparticle Catalysts for Fuel Cell Reactions. *Adv. Funct. Mater.*, 2010, **20**, P. 1224–1231.

[37] Lordi V., Yao N., Wei J. Method for Supporting Platinum on Single-Walled Carbon Nanotubes for a Selective Hydrogenation Catalyst. *Chem. Mater.*, 2001, **13**, P. 733–737.

[38] Emmanuel J. Comparative Activity of Platinum and Gold Nanoparticles Catalysts for Carbon Monoxide Oxidation. *Ethiop. J. Sci. Technol.*, 2022, **15**, P. 155–172.

[39] Haynes C.A., Gonzalez R. Rethinking Biological Activation of Methane and Conversion to Liquid Fuels. *Nat. Chem. Biol.*, 2014, **10**, P. 331–339.

[40] Sartipi S., Makkee M., Kapteijn F., Gascon J. Catalysis Engineering of Bifunctional Solids for the One-Step Synthesis of Liquid Fuels from Syngas: A Review. *Catal. Sci. Technol.*, 2014, **4**, P. 893–907.

[41] Centi G., Perathoner S. Status and Gaps toward Fossil-Free Sustainable Chemical Production. *Green Chem.*, 2022, **24**, P. 7305–7331.

[42] Ketchie W.C., Murayama M., Davis R.J. Selective Oxidation of Glycerol over Carbon-Supported AuPd Catalysts. *J. Catal.*, 2007, **250**, P. 264–273.

[43] Limpachanangkul P., Liu L., Hunsom M., Piumsomboon P., Chalermsinsuwan B. Application of Bi_2O_3/TiO_2 Heterostructures on Glycerol Photocatalytic Oxidation to Chemicals. *Energy Reports*, 2022, **8**, P. 1076–1083.

[44] Coseri S., Biliuta G., Simionescu B.C., Stana-Kleinschek K., Ribitsch V., Harabagiu V. Oxidized Cellulose—Survey of the Most Recent Achievements. *Carbohydr. Polym.*, 2013, **93**, P. 207–215.

[45] Jin B., Yao G., Wang X., Ding K., Jin F. Photocatalytic Oxidation of Glucose into Formate on Nano TiO_2 Catalyst. *ACS Sustain. Chem. Eng.*, 2017, **5**, P. 6377–6381.

[46] Zhao H., Ding X., Zhang B., Li Y., Wang C. Enhanced Photocatalytic Hydrogen Evolution along with Byproducts Suppressing over Z-Scheme Cd_xZn_{1-x}S/Au/g-C_3N_4 Photocatalysts under Visible Light. *Sci. Bull.*, 2017, **62**, P. 602–609.

[47] Herrera-Beurnio M.C., López-Tenllado F.J., Hidalgo-Carrillo J., Martín-Gómez J., Estévez R., Urbano F.J., Marinas A. Glycerol Photoreforming for Photocatalytic Hydrogen Production on Binary and Ternary Pt-g-C_3N_4-TiO_2 Systems: A Comparative Study. *Catal. Today*, 2024, **430**, 114548.

Information about the authors:

Ksenia O. Potapenko – Boreskov Institute of Catalysis, SB RAS, Novosibirsk, 630090, Russia; ORCID 0000-0002-7868-340; potapenko@catalysis.ru

Egor E. Aydakov – Boreskov Institute of Catalysis, SB RAS, Novosibirsk, 630090, Russia; ORCID 0000-0002-7730-765; e.ajdakov@g.nsu.ru

Evgeny Y. Gerasimov – Boreskov Institute of Catalysis, SB RAS, Novosibirsk, 630090, Russia; ORCID 0000-0002-3230-333; gerasimov@catalysis.ru

Ekaterina A. Kozlova – Boreskov Institute of Catalysis, SB RAS, Novosibirsk, 630090, Russia; ORCID 0000-0001-8944-766; kozlova@catalysis.ru

Conflict of interest: the authors declare no conflict of interest.